Geochemical Perspectives Letters

Copper isotope fractionation during asteroid core solidification

P. Ni[1,2*], Y. Zhan[3*], N.L. Chabot[4], C.J. Ryan[5], K. Zhu[6], N.X. Nie[7], S.B. Shirey[2], A. Shahar[2]

https://doi.org/10.7185/geochemlet.2432

Abstract

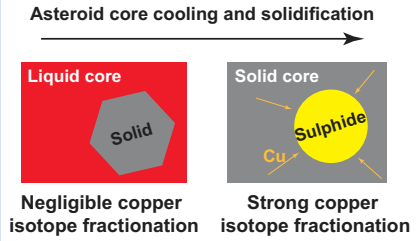

Moderately volatile elements (MVE) and their isotopic compositions are powerful tools to understand the origin of volatiles on terrestrial planets, including Earth. The $^{65}Cu/^{63}Cu$ ratio of Cu, one of the MVEs, has been found to be relatively high in the bulk silicate Earth (BSE), which potentially was caused by either evaporative loss or partitioning into Earth's inaccessible core. Iron meteorites are the accessible cores of differentiated planetesimals whose creation involved processes similar to Earth's in the early Solar System. Measurements of their Cu isotope composition currently yield a large range of values that reveal little about core-forming processes. Here, we determine the equilibrium Cu isotope fractionation between solid and liquid metal and quantify the partitioning of Cu between troilite and metal, showing that the latter is a more significant factor in fractionating the Cu isotopes when planetesimal cores cool. Our experiments also call for verification of existing data for equilibrium Cu isotope fractionation between silicate–sulphide and silicate–metal to support current models using sulphide segregation to explain the heavy Cu isotope enrichment in bulk silicate Earth and Moon.

Received 4 April 2024 | Accepted 15 July 2024 | Published 13 August 2024

Introduction

The terrestrial planets in our Solar System are vastly different from each other in internal structure and composition due to their distinct accretion and formation histories. Earth, when compared with the bulk Solar System composition as represented by the CI chondrites, exhibits a prominent depletion in moderately volatile elements, such as alkali elements, Cu, and Zn (McDonough and Sun, 1995). With a half condensation temperature of ~1030 K (Lodders, 2003; Wood *et al.*, 2019), Cu is one of the moderately volatile elements that could be susceptible to evaporative loss during the early stages of Earth accretion. On the other hand, Cu is also a moderately siderophile element (*e.g.*, Mahan *et al.*, 2018), indicating that its depletion in the Bulk Silicate Earth (BSE) could be due to core formation.

One potential way to understand the relative importance of the above two effects on Cu abundance in the BSE is to examine Cu isotope fractionation. Measurements of mid-ocean ridge basalts, ocean island basalts, komatiites, and peridotites defined a robust and precise BSE $\delta^{65}Cu$ (defined as the per mil difference in $^{65}Cu/^{63}Cu$ with respect to NIST SRM 976) value of 0.07 ± 0.10 ‰ (2 s.d.), significantly heavier than the estimated initial bulk Earth composition of −0.24 ± 0.09 ‰ (2 s.d.) based on chondrites (Savage *et al.*, 2015).

Despite the potential application of Cu isotopes to tracing planetary processes experienced by Earth, experimental studies on equilibrium Cu isotope fractionation are limited to only a few studies on silicate–metal and silicate–sulphide fractionation. These studies found limited fractionation between silicate melt and metallic liquid, but relatively large fractionations between silicate melt and sulphide liquid (up to 0.33 ‰, Xia *et al.*, 2019; ~1 ‰, Savage *et al.*, 2015), leading the authors to conclude that late segregation of a sulphide-rich liquid to the core has contributed to the heavy Cu isotope composition of the BSE (Savage *et al.*, 2015), and the bulk silicate Moon (BSM) (Xia *et al.*, 2019).

Core crystallisation is another process commonly experienced by differentiated asteroids and terrestrial bodies. Recent experiments by Ni *et al.* (2020) demonstrated that core crystallisation could introduce Fe isotope fractionation due to solid metal–liquid metal differentiation. This fractionation trend was observed in magmatic iron meteorites originated from the metallic cores of differentiated extinct asteroids (Ni *et al.*, 2020). Compiled copper isotope data of iron meteorites show large variations in their $\delta^{65}Cu$ from −6 ‰ to +1 ‰ (Figure 1), raising the

1. Department of Earth, Planetary, and Space Sciences, University of California, Los Angeles, CA 90095, USA
2. Earth and Planets Laboratory, Carnegie Institution for Science, Washington, DC 20015, USA
3. Department of Earth and Environmental Sciences, The Chinese University of Hong Kong, Shatin, N.T., Hong Kong
4. Johns Hopkins University Applied Physics Laboratory, Laurel, MD 20723, USA
5. Applied Research Laboratory, The Pennsylvania State University, University Park, PA 16801, USA
6. Bristol Isotope Group, School of Earth Sciences, University of Bristol, Bristol BS8 1RJ, United Kingdom
7. Department of Earth, Atmospheric, and Planetary Sciences, Massachusetts Institute of Technology, Cambridge, MA 02139, USA
* Corresponding authors (e-mail: pengni@epss.ucla.edu, yanzhan@cuhk.edu.hk)

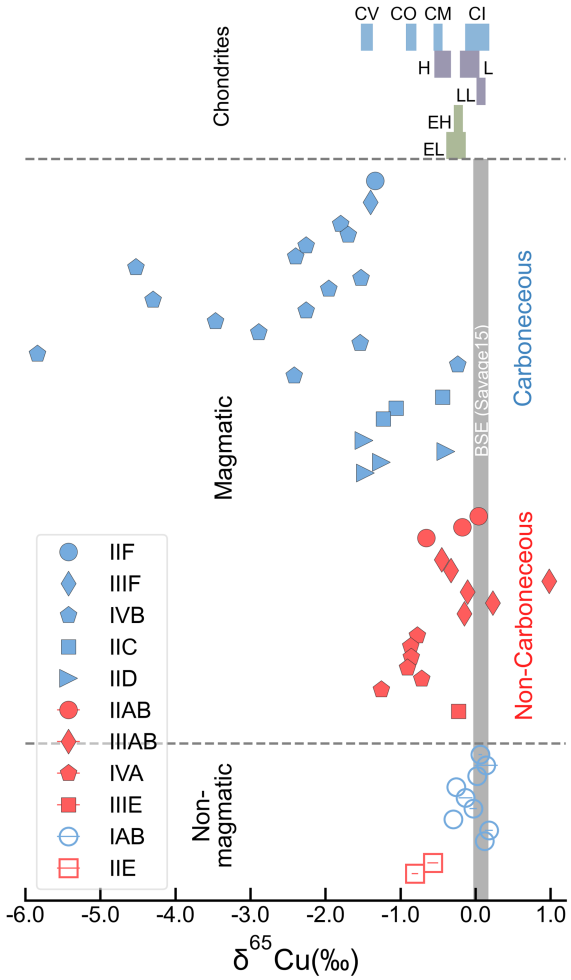

Figure 1 Copper isotope data for chondrites and iron meteorites. Data for different types of chondrites from Savage *et al.* (2015) and iron meteorites from Luck *et al.* (2005), Bishop *et al.* (2012), and Chen *et al.* (2016) are plotted. The bulk silicate Earth (BSE) composition is from Savage *et al.* (2015).

need to quantify the effect of core crystallisation on causing the variation. In this study, we conducted solid–liquid metal equilibrium experiments to constrain the degree of Cu isotope fractionation during core crystallisation in iron meteorite parent bodies. The experimental data are combined with a kinetic model to explain Cu isotope variations in iron meteorites. Our results are also used to indirectly assess existing Cu isotope exchange experiments that suggested a late-stage sulphide segregation in causing the bulk silicate Earth and Moon to be heavy in Cu isotopic composition.

Methods

Solid–liquid metal equilibrium experiments were conducted at the Johns Hopkins University Applied Physics Laboratory to simulate the core crystallisation process following the approach in Chabot *et al.* (2017) utilising vacuum-sealed silica tubes and vertical furnaces. Major element composition of the phases was analysed with a JEOL 8530F electron microprobe at the Carnegie Institution for Science. The quenched solid and liquid metal phases were sampled for Cu isotope measurements using a micromill equipped with tungsten carbide drill bits. Column purification of Cu was performed using in-house custom-made quartz glass columns following the procedure previously reported by Ni *et al.* (2021). Isotopic compositions of the purified Cu solution of the solid and liquid metal phases were measured using a Nu Plasma II Multi-Collector ICP-MS at the Carnegie Institution for Science in wet plasma mode. Analyses were conducted using ERM-AE633 as the bracketing standard, and all isotope results are reported relative to NIST SRM 976 after correcting a −0.01 ‰ difference between ERM-AE633 and NIST SRM 976 (Moeller *et al.*, 2012):

$$\delta^{65}\mathrm{Cu} = \left[\left(^{65}\mathrm{Cu}/^{63}\mathrm{Cu}\right)_{\mathrm{Sample}} / \left(^{65}\mathrm{Cu}/^{63}\mathrm{Cu}\right)_{\mathrm{SRM976}} - 1\right] \times 1000\,‰.$$

Modelling of the partitioning, diffusion, and isotopic fractionation of Cu between metal and troilite grains in iron meteorites was performed assuming one-dimensional diffusion in spherical coordinates and an asymptotic cooling history. Details about the experimental and analytical methods and the kinetic model are available in the Supplementary Information.

Results and Discussion

A total of ten solid–liquid metal equilibrium experiments were conducted at 1260–1425 °C to study Cu isotope fractionation during iron meteorite core crystallisation. Sulphur content of the liquid metal was intrinsically controlled by the temperature following the Fe-Ni-S phase diagram (Hsieh and Chang, 1987), with higher sulphur in the liquid at lower temperatures. Microscopic images of one experiment (S20-Cu1) are shown in Figure S-1 as an example. The quenched sample charges show distinct regions of solid metal (Fe-Ni alloy) and liquid metal (Fe-Ni-S), the latter with characteristic dendritic textures formed during quench. The quenched liquid metal contains 0.8 to 3.3 wt. % Cu while the solid metal contains 0.3 to 0.6 wt. % Cu (Table S-1). Calculated Cu partition coefficients between the solid and liquid metal vary from 0.11 to 0.62 as a function of sulphur content, generally consistent with literature data (Figure S-2; Chabot and Jones, 2003; Chabot *et al.*, 2009).

Although the Cu partitioning data indicate chemical equilibrium between the solid and liquid metal, it was not the case for Cu isotope exchange. Copper isotopic difference between the solid and liquid metal phases in these ten experiments vary significantly from 0.35 ± 0.04 ‰ to 1.75 ± 0.08 ‰. Further investigation of the experimental data showed that isotopic equilibrium was only reached for high-sulphur experiments at temperatures lower than 1350 °C (S15-Cu1, S20-Cu1, S25-Cu1, S25-Cu2, S25-Cu3). For low-sulphur experiments at higher temperatures (S5-Cu1, S5-Cu3, S10-Cu1, S15-Cu2, S15-Cu6), Cu isotopic composition was significantly affected by evaporation of Cu to the interior of the vacuum-sealed quartz glass tube. The initial bulk δ^{65}Cu was 0.45 ± 0.02 ‰ as measured on the Cu powder used for doping the experiments and the starting mixture for S15-Cu1 (Table S-2). The low-sulphur, high-temperature experiments reached isotopic compositions as heavy as 1.39 ± 0.19 ‰ for the solid metal and 1.75 ± 0.08 ‰ for the liquid metal (Figure S-3). Evaporative loss of the Cu occurs primarily in the liquid metal with higher mobility for the elements, driving it towards heavier δ^{65}Cu compositions. Copper diffusion in the solid metal limits its isotopic exchange with the liquid metal, causing its Cu isotope composition to exhibit a lighter value. This is evidenced by duplicated sampling and analyses of the same experiments, which yielded identical δ^{65}Cu composition for the liquid metal but different compositions for the solid metal in both cases (S5-Cu1, S10-Cu1; Table S-2). The evaporative loss of Cu is further proved by measuring the acid leachate of the tube inner wall of the most affected experiment (S15-Cu2). The Cu leachate yielded an extremely light Cu isotopic composition of −1.51 ± 0.06 ‰,

consistent with light Cu being preferentially lost during evaporation and later condensed on the low-temperature end of the quartz glass tube.

Due to the complications caused by Cu evaporation, equilibrium Cu isotope fractionation data are limited to the low-temperature experiments with 20 wt. % or more sulphur in the liquid metal (Figure S-4). Isotopic equilibrium between the solid and liquid metal was assessed by: 1) a set of time-series experiments conducted at the lowest temperature (1260 °C) for durations of 1, 2.75, and 5 days; 2) departure of the bulk Cu isotopic composition from the estimated initial composition ($\delta^{65}Cu = 0.45‰$). The time-series experiments yielded fractionation factors within error from each other, suggesting that isotopic equilibrium was reached within one day at 1260 °C (Figure S-3). For the low-temperature experiments with 20 wt. % or more sulphur, the bulk $\delta^{65}Cu$ varies between 0.36 ± 0.04 ‰ and 0.69 ± 0.03 ‰, within ~0.2 ‰ from the estimated initial of 0.45 ± 0.02 ‰ (Table S-2). We suspect the offset to the light composition was the consequence of isotopic heterogeneity within the Cu powder used for doping the experiments because Cu evaporation would only drive the bulk composition toward heavy values. The shift toward the heavy composition can be attributed to either isotopic heterogeneity or a small degree of Cu evaporation that was compensated by sufficient diffusive re-equilibration.

With the above considerations, five of the ten experiments with sulphur contents over 20 wt. % can be concluded to have reached isotopic equilibrium. All five experiments gave Cu isotope fractionation factors of ~0 ‰, indicating limited fractionation between solid and liquid metal (Figure 2; Table S-2). With a weighted average of 0.01 ± 0.04 ‰ for $\Delta^{65}Cu_{solid\text{–}liquid\ metal}$ ($\Delta^{65}Cu_{solid\text{–}liquid\ metal} = \delta^{65}Cu_{solid\text{–}metal} - \delta^{65}Cu_{liquid\text{–}metal}$), crystallisation of the parent core of magmatic iron meteorites does not cause significant isotope fractionation in Cu. This is different from the case of Fe (Ni *et al.*, 2020), where fractionation of over 0.1 ‰ occurs throughout the core crystallisation process. Such a low $\Delta^{65}Cu_{solid\text{–}liquid\ metal}$ conclusively excludes core crystallisation as a potential source of large Cu isotope variations in magmatic irons (Figure 1).

Another process common to the parent bodies of all magmatic iron meteorites that could affect their Cu isotope composition is the diffusive exchange between Fe metal and troilite. This process occurs at much lower temperatures than core crystallisation and would be separate from it. As a chalcophile element, Cu tends to partition into the troilite phase, especially

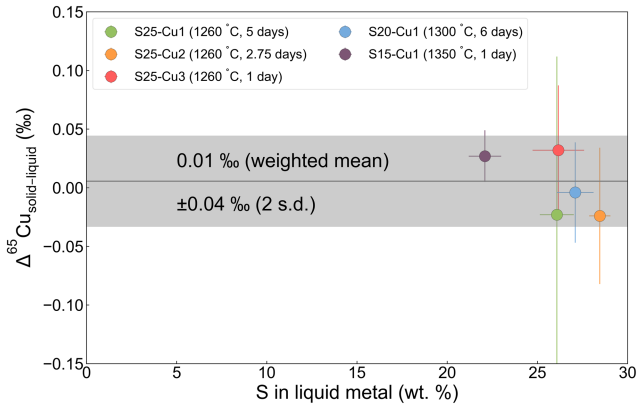

Figure 2 Equilibrium Cu isotope fractionation between solid and liquid metal during core crystallisation. A plot of all experimental data is available in Figure S-5. Error bars represent 2 standard deviations of the mean.

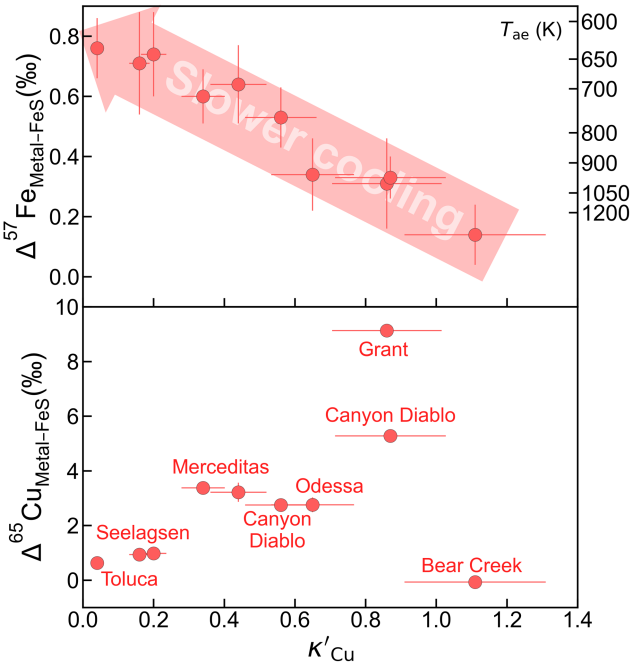

Figure 3 Iron and Cu isotope fractionation between metal and troilite in iron meteorites. Figure reproduced based on Williams and Archer (2011). The apparent partition coefficient of Cu is defined as $\kappa'_{Cu} = C_{FeS}(Cu)/C_{Meteorite}(Cu)$. Calculated apparent equilibrium temperature (T_{ae}) for Fe isotope fractionation is plotted on the right side of y-axis (see Supplementary Information).

as the temperature decreases. Direct measurements of troilite grains in iron meteorites found them to be as light as −9 ‰ in $\delta^{65}Cu$ (Williams and Archer, 2011). Such large fractionation can potentially explain the large Cu isotope variations seen in iron meteorites. According to the authors, this significant fractionation is likely the result of a kinetic process. As shown in Figure 3, Williams and Archer (2011) measured both Fe and Cu isotopes of troilite in iron meteorites. The fractionation of iron isotopes between the Fe-Ni alloy matrix and troilite was found to correlate with apparent Cu partition coefficient (calculated as Cu concentration of troilite divided by bulk meteorite Cu concentration) and kamacite bandwidth, which is related to cooling rate.

Iron meteorites that cooled down faster had less time to develop the Widmanstätten pattern and therefore tend to show narrower kamacite bands in general, although Ni and P concentrations also play a role. Chemically, a faster cooling rate would also limit the length scale of diffusion, "freezing" equilibrium Fe isotope fractionation and Cu partitioning that happened at higher temperatures. Iron meteorites with slower cooling rates, on the other hand, would have time to grow wider kamacite bands and allow for chemical re-equilibrium between the metal and troilite untill much lower temperatures. Our calculated apparent equilibrium temperatures based on Fe isotope fractionation factors from Dauphas *et al.* (2012) (see Supplementary Information) vary between 630 and 1200 K, which are generally consistent with the upper limit of troilite stability (Hsieh and Chang, 1987) and the lower end of Widmanstätten pattern nucleation (Yang and Goldstein, 2005).

Copper isotope compositions measured in the same samples (Williams and Archer, 2011) show much larger fractionations than possible equilibrium effects at magmatic temperatures (Figure 3). Unlike Fe, which is a primary component of both the metal and troilite phases in iron meteorites, Cu is a trace element that experiences significant redistribution between

these phases as it becomes more chalcophile upon cooling (Figure 3). Such redistribution requires mass transfer by diffusion in solid metal, potentially leading to large kinetic isotope fractionation. It has been proposed by Williams and Archer (2011) that the range of Cu isotope composition for troilites was the product of partial isotope equilibrium from an initial kinetically-caused, light signature.

We developed a quantitative model to simulate the diffusive exchange of Cu between the metal and troilite phases, aimed at assessing the extent of light Cu enrichment in the troilite from the cooling and redistribution of Cu within the iron meteorite parent body. The isotopic composition of the troilite is modelled as a function of cooling time scale (τ_c) and shown in Figure 4. The simulations were conducted assuming a troilite radius (a) of 2 mm, a metal matrix radius (b) of 40 mm, and a B value of −75,000 to characterise the temperature dependence of the partition coefficient (κ). At 1100–1200 K when troilites first form, Cu is approximately evenly distributed between metal and troilite, as evidenced by the highest apparent partition coefficient (κ) of ~1 in the meteorite Bear Creek (Figure 3) and solid metal–liquid metal–troilite equilibrium experiments (Shread *et al.*, 2024).

If an iron meteorite cooled down at extremely high cooling rates (*e.g.*, $\tau_c = 10$ years), the troilite exhibits only minor Cu isotopic fractionation due to the limited Cu exchange between the metal and troilite, "freezing" its elemental partition and Cu isotope fractionation at high-temperature equilibrium. This could be the case for the Bear Creek meteorite, which recorded a high Cu partition coefficient and low degrees of Fe and Cu isotope fractionation (Figure 3). With slightly longer cooling time scales, ranging from 0.1 to 100 ka, Cu will have time to diffuse from metal to sulphide. The diffusion front entering the troilite phase would be enriched with light Cu isotopes, quickly overwriting the initial Cu isotope signal that was dominated by equilibrium fractionation. This would decrease the δ^{65}Cu composition of the troilite to be as light as −10 ‰. At even longer cooling time scales, from 1 to 1000 Ma, the heavier Cu isotope in the metal matrix has more time to diffuse into the troilite, thus bringing its isotopic composition back to ~0 ‰, representing equilibrium fractionation (Figure S-5).

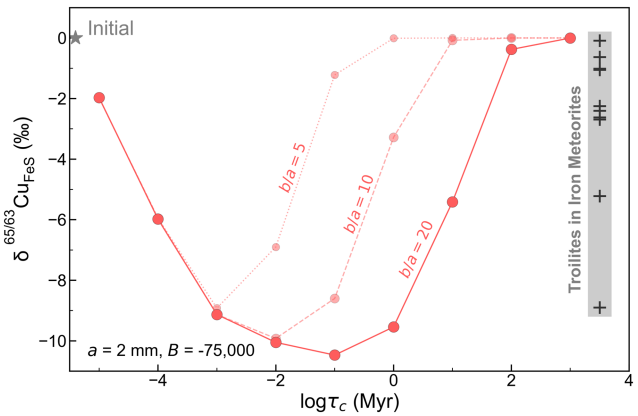

Figure 4 Modelled Cu isotope fractionation in troilite as a function of cooling time scale. The model was conducted assuming a troilite radius (*a*) of 2 mm, and a temperature dependence of the partition coefficient (*B*) of −75,000. Measured Cu isotope composition of troilites in iron meteorites is plotted on the right-hand side of the figure for comparison. Details of the model are described in the main text and in the Supplementary Information.

Simulations assuming smaller *b/a* ratios of 10 and 5 produced similar outcomes, albeit with the peak fractionation occurring at different cooling time scales. Our model offers a semi-quantitative explanation for the Cu isotope compositions observed in troilites from iron meteorites, demonstrating a non-monatomic dependence on cooling rate, as shown in Figure 4. The modelling results align with the observed trend turnover and the overall magnitude of fractionation depicted in Figure 3b.

Previous studies report a small positive fractionation between metal–silicate and relatively large negative fractionation between sulphide–silicate (Savage *et al.*, 2015; Xia *et al.*, 2019). Combining those results and assuming equilibrium conditions at ~1350 °C in all experiments would predict a 0.4 ‰ fractionation in δ^{65}Cu between metal and Ni-free sulphide, and 0.1 ‰ between metal and Ni-rich (~27 wt. %) sulphide. This contrasts with our measured fractionation of 0.01 ± 0.04 ‰ at 1260 °C. This discrepancy can be attributed to the lack of isotope equilibrium in previous experiments (see Supplementary discussion), a composition dependence that is not yet fully understood, or systematic differences between different experiment setups. A careful re-evaluation of Cu isotope fractionation will be necessary to support the current models of sulphide segregation in explaining the heavy Cu isotope composition of the bulk silicate Earth and the Moon.

Conclusion

We demonstrate through solid–liquid metal equilibrium experiments that core crystallisation of iron meteorite parent bodies does not result in measurable Cu isotope fractionation. Instead, the observed variations in Cu isotopes among iron meteorites are likely attributable to diffusive Cu enrichment into troilite from the metal matrix as the parent bodies cooled. Our quantitative model illustrates that this process can account for the observed magnitude of Cu isotope fractionation in troilite, as well as the general relationship between the fractionation and the cooling rate of iron meteorites. Interpreting the Cu isotope composition of iron meteorites' parent cores requires careful evaluation, correction, or possibly complete avoidance of the influence of troilites. Our experiments also illustrate the potential for isotopic disequilibrium, even when elemental partitioning appears to have reached equilibrium. This highlights the necessity of verifying existing experimental data on Cu isotope fractionation between silicate–metal and silicate–sulfide, which is crucial for substantiating the prevailing theory that late-stage sulphide segregation explains the Cu isotope composition of the bulk silicate Earth and the Moon.

Acknowledgements

We are grateful to M.F. Horan for assistance with column chemistry work and T.D. Mock for help with the MC-ICPMS measurements. We thank Steve Elardo, Kelsey Prissel, and an anonymous reviewer for their thoughtful comments and Francis McCubbin for editorial handling. This work is partly supported by NSF grant EAR-2025779 to AS and SBS and NASA Emerging Worlds Grant 80NSSC19K1613 to NLC.

Editor: Francis McCubbin

Additional Information

Supplementary Information accompanies this letter at https://www.geochemicalperspectivesletters.org/article2432.

Cite this letter as: Ni, P., Zhan, Y., Chabot, N.L., Ryan, C.J., Zhu, K., Nie, N.X., Shirey, S.B., Shahar, A. (2024) Copper isotope fractionation during asteroid core solidification. *Geochem. Persp. Let.* 31, 49–53. https://doi.org/10.7185/geochemlet.2432

References

Bishop, M.C., Moynier, F., Weinstein, C., Fraboulet, J.-G., Wang, K., Foriel, J. (2012) The Cu isotopic composition of iron meteorites. *Meteoritics and Planetary Science* 47, 268–276. https://doi.org/10.1111/j.1945-5100.2011.01326.x

Chabot, N.L., Jones, J.H. (2003) The parameterization of solid metal-liquid metal partitioning of siderophile elements. *Meteoritics and Planetary Science* 38, 1425–1436. https://doi.org/10.1111/j.1945-5100.2003.tb00248.x

Chabot, N.L., Saslow, S.A., McDonough, W.F., Jones, J.H. (2009) An investigation of the behavior of Cu and Cr during iron meteorite crystallization. *Meteoritics and Planetary Science* 44, 505–519. https://doi.org/10.1111/j.1945-5100.2009.tb00747.x

Chabot, N.L., Wollack, E.A., McDonough, W.F., Ash, R.D., Saslow, S.A. (2017) Experimental determination of partitioning in the Fe-Ni system for applications to modeling meteoritic metals. *Meteoritics and Planetary Science* 52, 1133–1145. https://doi.org/10.1111/maps.12864

Chen, H., Moynier, F., Humayun, M., Bishop, M.C., Williams, J.T. (2016) Cosmogenic effects on Cu isotopes in IVB iron meteorites. *Geochimica et Cosmochimica Acta* 182, 145–154. https://doi.org/10.1016/j.gca.2016.03.006

Dauphas, N., Roskosz, M., Alp, E.E., Golden, D.C., Sio, C.K., Tissot, F.L.H., Hu, M.Y., Zhao, J., Gao, L., Morris, R.V. (2012) A general moment NRIXS approach to the determination of equilibrium Fe isotopic fractionation factors: Application to goethite and jarosite. *Geochimica et Cosmochimica Acta* 94, 254–275. https://doi.org/10.1016/j.gca.2012.06.013

Hsieh, K.-C., Chang, Y.A. (1987) Thermochemical Description of the Ternary Iron-Nickel-Sulfur System. *Canadian Metallurgical Quarterly* 26, 311–327. https://doi.org/10.1179/cmq.1987.26.4.311

Lodders, K. (2003) Solar System Abundances and Condensation Temperatures of the Elements. *The Astrophysical Journal* 591, 1220. https://doi.org/10.1086/375492

Luck, J.-M., Othman, D.B., Albarède, F. (2005) Zn and Cu isotopic variations in chondrites and iron meteorites: Early solar nebula reservoirs and parent-body processes. *Geochimica et Cosmochimica Acta* 69, 5351–5363. https://doi.org/10.1016/j.gca.2005.06.018

Mahan, B., Siebert, J., Blanchard, I., Badro, J., Kubik, E., Sossi, P., Moynier, F. (2018) Investigating Earth's Formation History Through Copper and Sulfur Metal-Silicate Partitioning During Core-Mantle Differentiation. *Journal of Geophysical Research: Solid Earth* 123, 8349–8363. https://doi.org/10.1029/2018JB015991

McDonough, W.F., Sun, S.-s. (1995) The composition of the Earth. *Chemical Geology* 120, 223–253. https://doi.org/10.1016/0009-2541(94)00140-4

Moeller, K., Schoenberg, R., Pedersen, R.-B., Weiss, D., Dong, S. (2012) Calibration of the New Certified Reference Materials ERM-AE633 and ERM-AE647 for Copper and IRMM-3702 for Zinc Isotope Amount Ratio Determinations. *Geostandards and Geoanalytical Research* 36, 177–199. https://doi.org/10.1111/j.1751-908X.2011.00153.x

Ni, P., Chabot, N.L., Ryan, C.J., Shahar, A. (2020) Heavy iron isotope composition of iron meteorites explained by core crystallization. *Nature Geoscience* 13, 611–615. https://doi.org/10.1038/s41561-020-0617-y

Ni, P., Macris, C.A., Darling, E.A., Shahar, A. (2021) Evaporation-induced copper isotope fractionation: Insights from laser levitation experiments. *Geochimica et Cosmochimica Acta* 298, 131–148. https://doi.org/10.1016/j.gca.2021.02.007

Savage, P.S., Moynier, F., Chen, H., Shofner, G., Siebert, J., Badro, J., Puchtel, I.S. (2015) Copper isotope evidence for large-scale sulphide fractionation during Earth's differentiation. *Geochemical Perspectives Letters* 1, 53–64. https://doi.org/10.7185/geochemlet.1506

Shread, E.E., Chabot, N.L., Hamill, C.D., Ash, R.D., Corrigan, C.M. (2024) The crystallization of iron meteorites and the effect of troilite on trace element chemistry. *55th Lunar and Planetary Science Conference*, abstract #1024. https://www.hou.usra.edu/meetings/lpsc2024/pdf/1024.pdf

Williams, H.M., Archer, C. (2011) Copper stable isotopes as tracers of metal–sulphide segregation and fractional crystallisation processes on iron meteorite parent bodies. *Geochimica et Cosmochimica Acta 75*, 3166–3178. https://doi.org/10.1016/j.gca.2011.03.010

Wood, B.J., Smythe, D.J., Harrison, T. (2019) The condensation temperatures of the elements: A reappraisal. *American Mineralogist* 104, 844–856. https://doi.org/10.2138/am-2019-6852CCBY

Xia, Y., Kiseeva, E., Wade, J., Huang, F. (2019) The effect of core segregation on the Cu and Zn isotope composition of the silicate Moon. *Geochemical Perspectives Letters* 12, 12–17. https://doi.org/10.7185/geochemlet.1928

Yang, J., Goldstein, J.I. (2005) The formation of the Widmanstätten structure in meteorites. *Meteoritics and Planetary Science* 40, 239–253. https://doi.org/10.1111/j.1945-5100.2005.tb00378.x

Copper isotope fractionation during asteroid core solidification

P. Ni, Y. Zhan, N.L. Chabot, C.J. Ryan, K. Zhu, N.X. Nie, S.B. Shirey, A. Shahar

Supplementary Information

The Supplementary Information includes:

1. Solid-liquid metal equilibrium experiments for Cu

The solid-liquid metal equilibrium experiments were conducted at the Johns Hopkins University Applied Physics Laboratory following a similar approach as in Chabot *et al.* (2017). High-purity Fe, Ni, and FeS powders were mixed and doped with approximately 1 wt. % Cu powder. For experiments S25-Cu1, S25-Cu2, S25-Cu3, S15-Cu1, S10-Cu1, and S5-Cu1, a small amount of Ru, Os, and W were doped in the starting mixture for separate purposes (Table S-1). For each of the 10 experiments, appropriate amounts of the starting mixtures were weighed and sealed in a high-purity silica tube that was connected to vacuum. Experiments were conducted using a one-atmosphere vertical furnace at temperatures of 1260 to 1425 ºC. The duration of the experiments was between 1 and 6 days. At the end of the experiments, the silica tube was removed from the furnace and quenched in water. The experimental samples were subsequently recovered from the tube and mounted in epoxy for preservation. After being sliced into multiple sections using a diamond saw, cross sections of the sample were mounted in epoxy again and polished to achieve a smooth surface for analyses.

2. Electron microprobe analyses

Electron microprobe analyses were conducted to measure major element compositions of the experimental samples for Fe, Ni, S, and Cu at the Carnegie Institution for Science using a JEOL 8530 F electron microprobe. A 15 kV, 20 nA beam was defocused to 100 µm for the quenched solid and metal phases in the experiments. The large beam diameter was important to compensate for the chemical heterogeneities caused by the quench textures in the liquid metal phase, as shown in Figure S-1. The counting time was 30 s for Ni, Fe and Cu and

60 s for S. For each phase of the experiments, approximately 10 to 20 analyses were conducted and the errors were reported as two standard deviations of the mean. For the liquid metal phase, however, errors were reported as two standard errors of the mean to average out uncertainties caused by the dendritic quench textures.

3. Copper isotope analyses

The solid and liquid metal phases of the experiments were sampled using a Newwave micromill for Cu isotope analyses. The samples were cleaned in an ultrasonic bath of deionized water prior to drilling. A new tungsten carbide drill bit 300 to 700 µm in diameter was used for each phase to avoid cross-contamination. Each drill hole was 400 to 500 µm in depth. For phases with low concentrations of Cu, materials from multiple drill holes were combined to ensure the recovery of sufficient amount of Cu for analyses. A drop of Milli-Q water was placed at the target position before drilling to help collect the drilled particles with the surface tension of water. The drilled particles were suspended in the Milli-Q and transferred to a Teflon vial using a pipette. A few drops of Milli-Q water were placed near the drill site to help transfer the residual particles afterwards and the process was repeated multiple times. The sample surface was always cleaned with Milli-Q water and compressed air before being used for drilling the next phase. Since the liquid metal phases have higher concentrations of Cu, sampling of each experimental charge was always started with the solid metal and then the liquid metal. After micromill sampling, the drilled holes were examined with an optical microscope to ensure they only penetrated one phase as originally planned.

The drilled particles were dried down on a hot plate, and dissolved in 1 ml concentrated HCl + 0.5 ml concentrated HNO_3 on a hot plate for at least 24 hours. After complete dissolution was achieved, the sample was dried down and small amounts of concentrated HCl was added to the Teflon vials to drive away NO_3^- introduced during the dissolution. Chemical purification of Cu was performed using established lab procedures previously published in Ni *et al.* (2021). In-house custom-made quartz glass columns 0.4 cm in diameter were loaded with approximately 7.5 cm of BioRad AG1-X8 (200-400 mesh) resin for Cu purification. After being converted to the chloride form, dissolved samples were loaded on the column in 8 M HCl + 0.001% H_2O_2. Then 7 ml of 8 M HCl + 0.001% H_2O_2 was added to remove most of the matrix elements. The Cu fraction of the column was then collected by eluting 9 ml of 8 M HCl + 0.001% H_2O_2. The above procedure was repeated once to achieve cleaner separation of Cu from the matrix elements. Two milliliters of eluents before and after the Cu fraction of the column were collected separately to monitor any potential shift of the Cu peak and to ensure the recovery rate was >99%. The blank of the column procedure was 0.5 ng, significantly lower than the amount of Cu yielded in each sample (250 ng to 50 µg).

Copper isotope analyses were conducted using the Nu Plasma II at the Carnegie Institution for Science. The instrument was operated at low mass resolution in wet plasma mode. Samples and standards were diluted to 50 or 100 ppb in 0.4 M HNO_3 for analyses and the sensitivity was 25-40 V/ppm for ^{63}Cu. Each sample was analysed 4 to 10 times and each measurement consisted of 20 cycles with 4 s integrations. ERM-AE633 was used as the isotope standard for sample-standard bracketing to correct for instrumental mass bias. The measured Cu isotope ratios are reported relative to NIST SRM 976 after correcting a -0.01‰ difference between the two isotope standards (ERM-AE633 and NIST SRM 976, Moeller *et al.*, 2012):

$$\delta^{65}\mathrm{Cu}\ (‰) = \left[\left(^{65}\mathrm{Cu}/^{63}\mathrm{Cu}\right)_{\mathrm{Sample}}/\left(^{65}\mathrm{Cu}/^{63}\mathrm{Cu}\right)_{\mathrm{SRM976}} - 1\right] \times 1000$$
$$= \left[\left(^{65}\mathrm{Cu}/^{63}\mathrm{Cu}\right)_{\mathrm{Sample}}/\left(^{65}\mathrm{Cu}/^{63}\mathrm{Cu}\right)_{\mathrm{AE633}} - 1\right] \times 1000 + 0.01.$$

4. Calculating apparent equilibrium temperature for Fe isotope fractionation between metal and troilite

Apparent equilibrium temperatures for Fe isotope fractionation between metal and troilite in iron meteorites were calculated using published reduced partition function ratio for α-Fe (bcc) and troilite (Dauphas *et al.*, 2012, 2017). The equilibrium fractionation factor for α-Fe (bcc) was calculated using:

$$1000\ln\beta_{\alpha\text{-Fe}}(^{56}\text{Fe}/^{54}\text{Fe}) = 0.49970 \times 10^6/T^2 - 1.14240 \times 10^9/T^4,$$

while that for troilite was using:

$$1000\ln\beta_{\text{troilite}}(^{56}\text{Fe}/^{54}\text{Fe}) = 0.29101 \times 10^6/T^2 - 0.63530 \times 10^9/T^4.$$

In the above equations T is the temperature in K.

Equilibrium isotope fractionation between metal and troilite was subsequently calculated via:

$$\Delta_{56/54}(\alpha\text{-Fe/troilite}) = 1000\ln\beta_{\alpha\text{-Fe}}(^{56}\text{Fe}/^{54}\text{Fe})\text{-}1000\ln\beta_{\text{troilite}}(^{56}\text{Fe}/^{54}\text{Fe}).$$

And $\Delta_{57/54}(\alpha\text{-Fe/troilite})$ was calculated assuming mass-dependent fractionation of the three isotopes of iron following the equilibrium fractionation law (Young *et al.*, 2002):

$$\Delta_{57/54}(\alpha\text{-Fe/troilite}) = (1/M_{54} - 1/M_{57})/(1/M_{54} - 1/M_{56}) \times \Delta_{56/54}(\alpha\text{-Fe/troilite})$$
$$= 1.475 \times \Delta_{56/54}(\alpha\text{-Fe/troilite}).$$

The calculated apparent equilibrium temperatures (T_{ae}) are plotted in Figure 3.

5. Lessons learned for equilibrium isotope fractionation experiments

Our experiments have profound implications for equilibrium isotope fractionation experiments. First, our data unambiguously show that elemental equilibrium cannot be used to indicate isotope equilibrium. As shown in Figure S-2, all 10 experiments yielded Cu partition coefficients consistent with literature data. But careful evaluation of isotopic equilibrium demonstrated that the five experiments at higher temperatures have experienced evaporative Cu loss, leading to kinetic isotope fractionation. Copper was lost from the liquid metal during evaporation, causing Cu to diffuse from solid metal into liquid metal to maintain equilibrium. But this was limited by Cu diffusion in solid metal and caused the measured partition coefficients to be on the high end of the data (Figure S-2). This process led to limited departure from equilibrium Cu partitioning that is hard to distinguish from experimental errors, but the effect on Cu isotope fractionation is quite significant. The diffusive reequilibrium caused the liquid metal to become higher in ^{65}Cu/^{63}Cu ratio over time and the solid metal to show isotopic heterogeneity (Figure S-4, Table S-2). This finding indicates the importance of the closed system test for isotope equilibrium experiments. If a sink or a source of the target element exists in the system, it might reach a steady state instead of true equilibrium. At such steady states, element partition could still reach near-equilibrium, but isotope exchange would be dominated by kinetic fractionation.

Second, for isotope systems like Cu that only contain two stable isotopes, the "three-isotope" technique cannot be applied to test for isotopic equilibrium (Shahar *et al.*, 2017), making it especially important to check for closed system behavior of the element and conduct time-series experiments. Based on a combination of both tests, we were able to distinguish experiments in our study that did not reach isotope equilibrium. Unfortunately, these methods have not been specifically employed in previous experiments for equilibrium Cu isotope fractionation (Savage *et al.*, 2015; Xia *et al.*, 2019), making it less convincing that isotopic equilibrium has been reached in these experiments. The exact cause for the Cu loss trend in our non-equilibrated experiments (Figure S-4) is unclear, but we suspect it was the consequence of multiple factors: 1) effect of temperature and sulphur content on Cu volatility; 2) duration of the experiment; and 3) surface area of the liquid metal exposed for evaporation.

Third, our data demonstrate how deceiving trends could appear for experiments that are dominated by kinetic isotope fractionation. As plotted in Figure S-5, the five experiments affected by evaporative Cu loss appear to have a linear correlation between Δ^{65}Cu and S content of the liquid metal, except for one data point that falls slightly off the trend (S15-Cu2). Note that this trend is completely artificial but could misguide ones to believe that these experiments have reached isotopic equilibrium. In fact, it is quite possible for kinetically controlled isotope exchange experiments to show temperature dependence. This is because diffusion and chemical reaction rates are also temperature dependent. For a non-equilibrium system, it is possible that it reaches closer to equilibrium fractionation at higher temperatures but further away from equilibrium at lower temperatures. This temperature effect could lead to a larger apparent isotopic fractionation between two phases at lower temperatures but a smaller fractionation at higher temperatures, which is coincidentally the expectation for equilibrium fractionation. Therefore, judging whether experiments have reached isotopic equilibrium based on the final trend of the data could be misguiding.

Overall, our experiments strongly support the necessity of independently verifying isotopic equilibrium for isotope exchange experiments. For isotope systems that contain only two stable isotopes, it is especially important to test for closed system behavior of the target element and conduct time series experiments to check for isotopic equilibrium.

6. Modelling of Cu redistribution between metal and troilite during cooling of the iron meteorite parent body

Assuming a spherical troilite with fixed radius of a exchanging Cu with matrix metal in a finite radius of b, the governing equation describing Cu diffusion in one-dimensional spherical coordinate is:

$$\frac{\partial C}{\partial t} = \frac{D}{r^2}\frac{\partial}{\partial r}\left(r^2\frac{\partial C}{\partial r}\right)|_{a\le r\le b},$$

with boundary conditions of:

$$\frac{\partial C}{\partial r}|_{r=b} = 0,$$

$$C(t)|_{r=a} = \kappa C_{FeS}(t),$$

$$\text{and } dC_{FeS} = \frac{\int_a^b 4\pi r^2 \rho_{Metal}(C-C_0)dr}{4/3\pi a^3 \rho_{FeS}}.$$

In the above equation, D is the diffusivity, r is the radial distance, C is the concentration in the metal matrix, κ is Cu partition coefficient between metal and troilite, ρ_{Metal} and ρ_{FeS} are densities of metal and troilite, C_0 is the initial concentration in metal, and C_T is the concentration in the troilite and assumed to be homogeneous. Copper diffusion in sulphide (Cherniak, 2010) is orders of magnitude faster than in metal (Salje and Feller-Kniepmeier, 1977), making it possible to reach a homogeneous composition in the troilite when exchanging Cu with the metal matrix.

The key parameters needed to solve the above equations are the diffusivity of Cu (D) and the Cu partition coefficient (κ), which are both functions of temperature. Copper diffusivity in iron metal has been experimentally determined (Salje and Feller-Kniepmeier, 1977) and re-fitted to be:

$$D = D_0 \exp\left(-\frac{E_0}{RT}\right) = 0.03 \exp\left(\frac{283675\ J/mol}{RT}\right) m^2/s.$$

In the above equation, D_0 is the pre-exponential term in m^2/s, E_0 is the activation energy for diffusion, and R is the gas constant which equals 8.314 J/mol/K.

Experimental data on Cu partitioning between metal and troilite (κ) are limited. A recent study found κ to be 1 for Cu at the solid metal-liquid metal-troilite cotectic (Shread *et al.*, 2024), which also agrees with the observed apparent κ in iron meteorites with high cooling rates (Figure 3). Therefore, we fix κ = 1 at 1200 K and convert Eq. (3) into the form of:

$$\ln\kappa = -\frac{B}{T_0} + \frac{B}{T},$$

in which T_0 = 1200 K and B is an adjustable parameter that determines how strongly κ depends on temperature. At $T = T_0$, κ always have a value of 1 regardless the value of B.

The thermal history of the iron meteorite parent bodies is simulated using the asymptotic cooling model:

$$T = \frac{T_0 - T_c}{1 + \frac{t}{\tau_c}} + T_c,$$

where T_0 is the initial temperature, T_c is the terminal temperature, t is time, and τ_c is the cooling time scale. In order to calculate isotopic fractionation of ^{63}Cu and ^{65}Cu, they were assumed to have the same partition coefficient between metal and troilite (i.e., $\kappa_{63\mathrm{Cu}} = \kappa_{65\mathrm{Cu}} = \kappa_{\mathrm{Cu}}$, no equilibrium isotope fractionation), but different diffusivities as a function of their mass:

$$\frac{D_{63Cu}}{D_{65Cu}} = \left(\frac{M_{65}}{M_{63}}\right)^{\beta} = \left(\frac{64.927789}{62.929597}\right)^{\beta}.$$

In the above equation, β ($0 \leq \beta \leq 0.5$) is an empirical parameter that describes how the two isotopes of Cu fractionate by diffusion. Existing data for Cu diffusion in Al, Cu, CuZn, Li, and Pb yielded a large range of β values from 0.1 to 0.45, making it difficult to predict how Cu would behave in Fe metal. Therefore, a β value of 0.5 is used to explore the maximum effect of kinetic fractionation for Cu isotopes.

In each simulation, the concentration profiles of ^{63}Cu and ^{65}Cu were solved independently and their ratios along the profile were compared with the initial ratio to obtain isotopic fractionation expressed in delta notations:

$$\delta^{65}\mathrm{Cu}\,(r,t) = \left(\frac{^{65}\mathrm{Cu}(r,t)/^{63}\mathrm{Cu}(r,t)}{(^{65}\mathrm{Cu}/^{63}\mathrm{Cu})_0} - 1\right) \times 1000‰,$$

where $(^{65}\mathrm{Cu}/^{63}\mathrm{Cu})_0$ is the initial Cu isotopic ratio, which is assumed to be homogenous throughout the system at t = 0.

A list of all parameters required to reproduce our model is provided in Table S-3. A troilite radius of 2 mm was chosen for the model based on the average size of troilite grains analysed in Williams and Archer (2011). The effective matrix radius was assumed to be 5, 10, or 20 times that of the troilite. The value of B for the temperature dependence of the partition coefficient is unknown and remains a large uncertainty of the model. A B value of -75,000 was arbitrarily chosen based on test model runs that showed the maximum effect of kinetic fractionation.

With the above boundary conditions and initial conditions, the governing one-dimensional diffusion equation was solved numerically using a COMSOL Multiphysics 6.0. The model was first performed at a fixed temperature for a given duration to benchmark with the analytical solution, before being applied to the temperature-dependent situations.

Supplementary Tables

Table S-1 Run conditions and chemical compositions for all ten solid-liquid metal experiments. Concentrations are in wt. %. Errors are given in 2 standard deviations for the solid metal, but in 2 standard errors for the liquid metal phase to account for the chemical heterogeneity caused by quench textures.

Exp #	Phase	*T* (°C)	*t* (days)	Fe	Ni	S	Cu	Total
S25-Cu1*	Solid	1260	5	86.39±0.41	12.14±0.12	0.04±0.01	0.36±0.03	98.58±0.43
	Liquid			62.68±0.90	7.35±0.46	26.08±0.94	1.68±0.14	96.11±1.38
S25-Cu2*	Solid	1260	2.75	85.91±0.55	12.49±0.13	0.03±0.01	0.37±0.02	98.43±0.57
	Liquid			59.93±0.66	7.09±0.36	28.46±0.59	3.31±0.25	95.47±0.99
S25-Cu3*	Solid	1260	1	82.34±0.86	11.95±0.21	0.04±0.01	0.36±0.04	94.33±0.89
	Liquid			59.68±1.38	7.15±0.41	26.16±1.43	2.63±0.25	93.00±2.04
S20-Cu1*	Solid	1300	6	86.12±0.51	12.30±0.09	0.03±0.01	0.37±0.05	98.46±0.52
	Liquid			62.08±0.83	7.63±0.50	27.10±1.01	2.46±0.13	96.81±1.41
S15-Cu1*	Solid	1350	1	86.73±0.43	12.00±0.09	0.04±0.01	0.49±0.05	98.76±0.44
	Liquid			65.49±1.19	9.16±0.28	22.09±0.90	1.68±0.14	96.73±1.52
S15-Cu2	Solid	1370	1	89.15±0.67	9.77±0.14	0.05±0.01	0.44±0.04	99.40±0.34
	Liquid			74.00±0.23	9.32±0.09	14.86±0.33	1.35±0.07	99.53±0.42
S15-Cu6	Solid	1380	2.75	90.62±0.47	9.00±0.07	0.05±0.02	0.46±0.03	100.13±0.26
	Liquid			79.48±0.28	8.93±0.05	10.90±0.25	1.02±0.03	100.33±0.38
S10-Cu1*	Solid	1380	4	87.25±0.65	10.52±0.16	0.04±0.02	0.47±0.04	97.81±0.67
	Liquid			73.46±0.56	10.08±0.04	14.41±0.33	1.39±0.06	97.94±0.66
S5-Cu1*	Solid	1425	1	88.71±0.25	10.10±0.13	0.04±0.01	0.60±0.08	98.84±0.28
	Liquid			83.38±0.44	10.80±0.07	4.39±0.49	0.97±0.06	98.57±0.66
S5-Cu3	Solid	1400	1	88.32±0.76	9.86±0.08	0.04±0.01	0.46±0.04	98.68±0.41
	Liquid			81.54±0.30	10.29±0.06	6.26±0.39	0.80±0.06	98.90±0.50

*These experiments were doped with a few weight percent of Os, W, and Ru for separate purposes. The totals of the solid metal and liquid metal phases in these experiments do not account for these three elements and could hence be significantly lower than 100 wt. %.

Table S-2 Copper isotope compositions for the solid–liquid metal equilibrium experiment products. Errors are reported in two standard errors of 4 to 10 analyses.

Exp #	Phase	*T* (°C)	*t* (days)	δ^{65}Cu (‰)	n	$\Delta^{65}Cu_{sol\text{-}liq\ metal}$ (‰)
S25-Cu1	Solid Liquid	1260	5	0.43±0.07 0.46±0.10	5 4	-0.02±0.14
S25-Cu2	Solid Liquid	1260	2.75	0.47±0.04 0.49±0.04	10 9	-0.02±0.06
S25-Cu3	Solid Liquid	1260	1	0.38±0.04 0.35±0.04	10 10	0.03±0.06
S20-Cu1	Solid Liquid	1300	6	0.68±0.03 0.69±0.02	8 8	0.00±0.04
S15-Cu1	Solid Liquid	1350	1	0.65±0.03 0.62±0.04	8 8	0.03±0.06
S15-Cu2	Solid Liquid Tube leachate	1370	1	1.39±0.19 1.75±0.08 -1.51±0.06	4 4 8	*Not equilibrated*
S15-Cu6	Solid Liquid	1380	2.75	0.92±0.08 1.29±0.11	4 4	*Not equilibrated*
S10-Cu1	Solid *duplicate* Liquid *duplicate*	1380	4	0.81±0.03 0.91±0.02 1.60±0.05 1.54±0.03	6 4 6 4	*Not equilibrated*
S5-Cu1	Solid *duplicate* Liquid *duplicate*	1425	1	0.54±0.04 0.72±0.02 0.75±0.02 0.79±0.03	6 4 6 4	*Not equilibrated*
S5-Cu3	Solid Liquid	1400	1	0.71±0.06 0.92±0.05	8 8	*Not equilibrated*
S15-Cu1 initial powder	*N/A*	*N/A*	*N/A*	0.44±0.02	10	*N/A*
Cu powder	*N/A*	*N/A*	*N/A*	0.45±0.02	8	*N/A*

Table S-3 List of parameters and their values used in the model for Cu exchange between metal–troilite and the consequences for Cu isotope fractionation during cooling of iron meteorite parent bodies.

Symbol	Description	Value	Unit
D_0	Pre-exponential factor for Cu diffusivity in iron metal	0.03	m^2/s
E_0	Activation Energy for Cu diffusivity in iron metal	283675	J/mol
T_0	Initial temperature	1200	K
T_c	Terminal temperature	600	K
C_0	Initial concentration of Cu in the metal matrix	1	Dimensionless
ρ_{FeS}	Density of the troilite	4610	kg/m^3
ρ_{Metal}	Density of iron metal	7870	kg/m^3
a	Radius of the troilite grain	2	mm
b	Radius of the iron meteorite matrix exchanging with troilite	10, 20, 40	mm
B	Coefficient for temperature dependence of κ	-7.5×10^4	K
β	Factor for Cu isotope fractionation by	0.5	Dimensionless
τ_c	Cooling time scale	0.001 to 100	Myr

Supplementary Figures

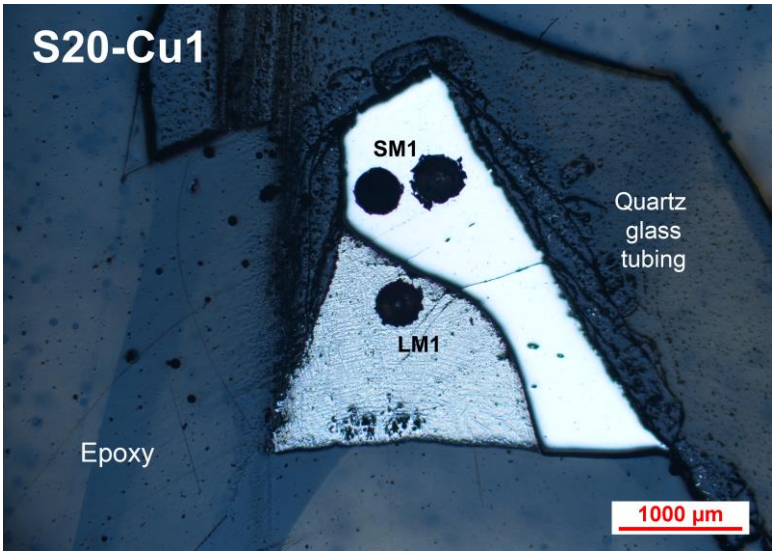

Figure S-1 Microscopic image of an experimental charge (S20-Cu1) after being sliced, preserved in epoxy, and sampled by a micromill for Cu isotope analyses. The drill holes on the solid metal and quenched liquid metal are marked as "SM1" and "LM1", respectively. The quenched liquid metal shows dendritic quench textures typical of this type of experiments.

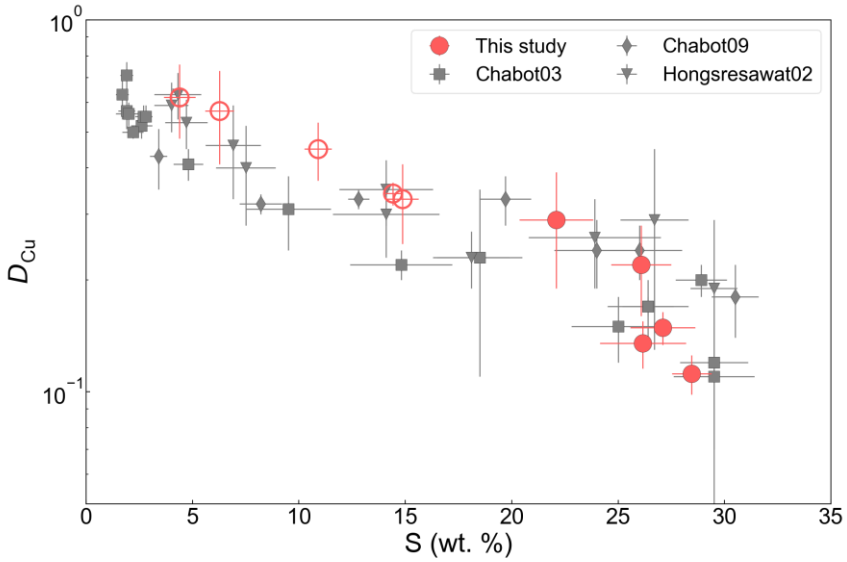

Figure S-2 Measured Cu partition coefficients between solid metal and liquid metal in this study compared with literature data. All 10 experiments appear to have reached equilibrium in Cu partitioning between the two phases. Experiments that show isotopic disequilibrium are plotted in open symbols. Sulphur content on the x-axis refers to that of the liquid metal. Error bars represent one standard deviation. Literature data are from (Chabot and Jones, 2003; Chabot *et al.*, 2009).

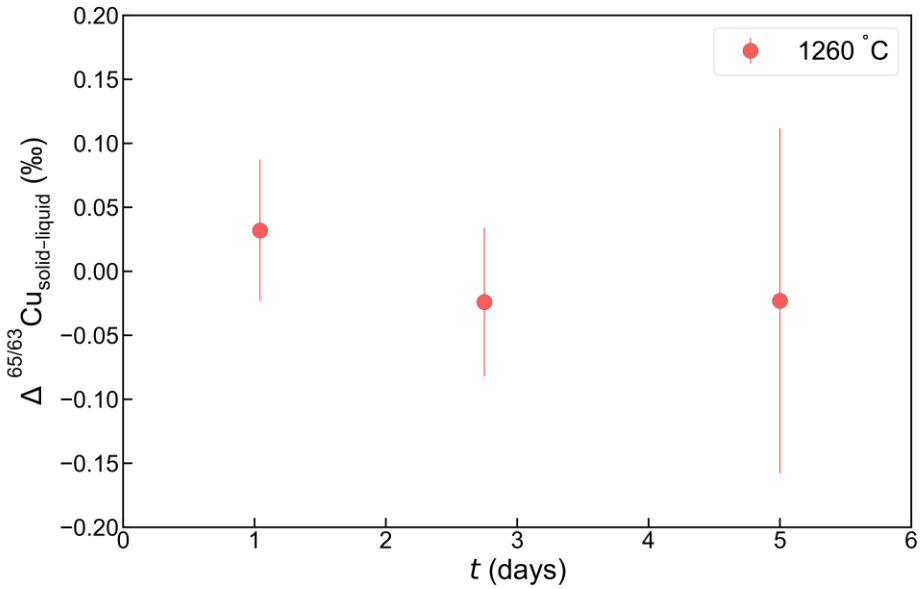

Figure S-3 Copper isotope fractionation factor for the time-series of experiments conducted at 1260 ºC. All three experiments yielded consistent results within error from each other, indicating that Cu isotope fractionation reached equilibrium within 1 day at 1260 ºC.

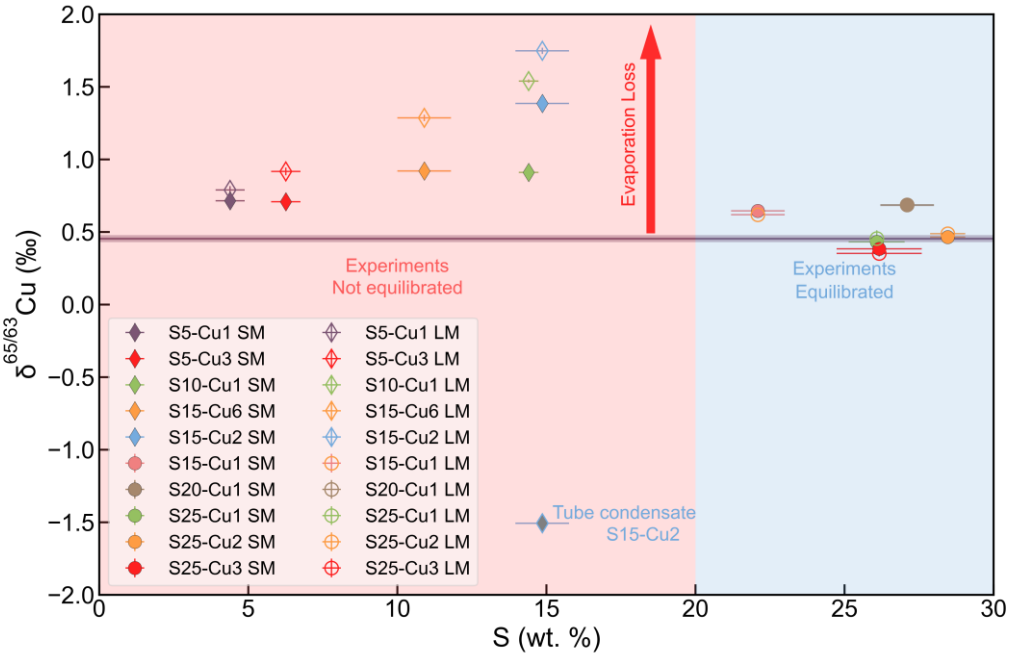

Figure S-4 Copper isotope composition of the liquid metal and solid metal for all 10 experiments conducted in this study. Initial bulk Cu composition is estimated to be 0.45 ‰ based on the Cu powder used for doping the experiments and plotted on the figure as a horizontal line.

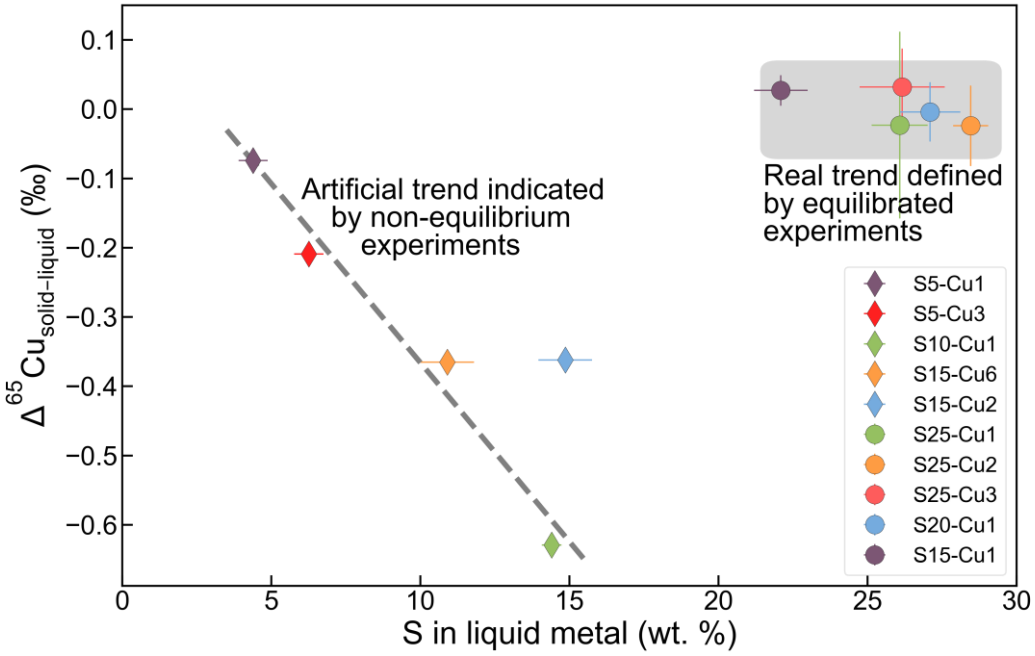

Figure S-5 Apparent Cu isotope fractionation between the solid metal and liquid metal phases directly calculated from all experiments.

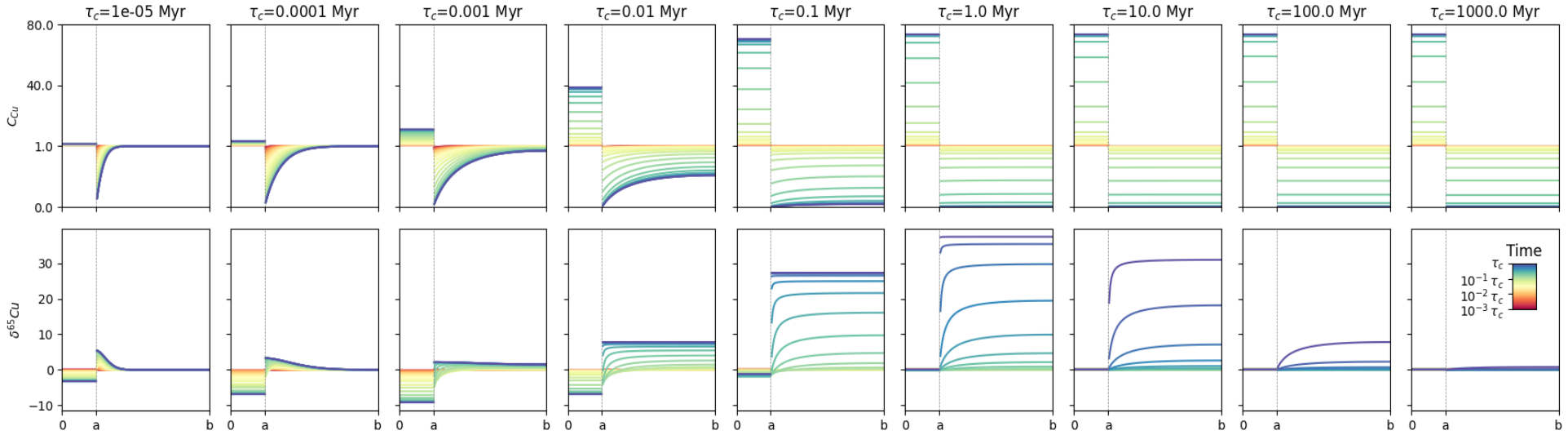

Figure S-6 Evolution of the Cu concentration and isotopic composition profiles in the troilite and metal matrix under different cooling time scales. The boundary between troilite and metal is marked using a dashed vertical curve. Copper concentration is unitless while δ^{65}Cu is in per mil. The profiles in each column show the results from models with different cooling rates from extremely high (τ_c = 10 yr) to extremely low (τ_c = 1 Gyr) values. The model assumes a troilite radius of 2 mm, metal matrix radius of 10 mm, and a temperature dependence for partition coefficient (B) of -75,000. The β value used for Cu diffusion is 0.5. More details about the model are available in the supplementary discussion.

Supplementary Information References

Chabot, N.L., Jones, J.H. (2003) The parameterization of solid metal-liquid metal partitioning of siderophile elements. *Meteoritics and Planetary Science* 38, 1425–1436. https://doi.org/10.1111/j.1945-5100.2003.tb00248.x

Chabot, N.L., Saslow, S.A., McDonough, W.F., Jones, J.H. (2009) An investigation of the behavior of Cu and Cr during iron meteorite crystallization. *Meteoritics and Planetary Science* 44, 505–519. https://doi.org/10.1111/j.1945-5100.2009.tb00747.x

Chabot, N.L., Wollack, E.A., McDonough, W.F., Ash, R.D., Saslow, S.A. (2017) Experimental determination of partitioning in the Fe-Ni system for applications to modeling meteoritic metals. *Meteoritics and Planetary Science* 52, 1133–1145. https://doi.org/10.1111/maps.12864

Cherniak, D.J. (2010) Diffusion in Carbonates, Fluorite, Sulfide Minerals, and Diamond. *Reviews in Mineralogy and Geochemistry* 72, 871–897. https://doi.org/10.2138/rmg.2010.72.19

Dauphas, N., Roskosz, M., Alp, E.E., Golden, D.C., Sio, C.K., Tissot, F.L.H., Hu, M.Y., Zhao, J., Gao, L., Morris, R.V. (2012) A general moment NRIXS approach to the determination of equilibrium Fe isotopic fractionation factors: Application to goethite and jarosite. *Geochimica et Cosmochimica Acta* 94, 254–275. https://doi.org/10.1016/j.gca.2012.06.013

Dauphas, N., John, S.G., Rouxel, O. (2017) Iron Isotope Systematics. *Reviews in Mineralogy and Geochemistry* 82, 415–510. https://doi.org/10.2138/rmg.2017.82.11

Moeller, K., Schoenberg, R., Pedersen, R.-B., Weiss, D., Dong, S. (2012) Calibration of the New Certified Reference Materials ERM-AE633 and ERM-AE647 for Copper and IRMM-3702 for Zinc Isotope Amount Ratio Determinations. *Geostandards and Geoanalytical Research* 36, 177–199. https://doi.org/10.1111/j.1751-908X.2011.00153.x

Ni, P., Macris, C.A., Darling, E.A., Shahar, A. (2021) Evaporation-induced copper isotope fractionation: Insights from laser levitation experiments. *Geochimica et Cosmochimica Acta* 298, 131–148. https://doi.org/10.1016/j.gca.2021.02.007

Salje, G., Feller-Kniepmeier, M. (1977) The diffusion and solubility of copper in iron. *Journal of Applied Physics* 48, 1833–1839. https://doi.org/10.1063/1.323934

Savage, P.S., Moynier, F., Chen, H., Shofner, G., Siebert, J., Badro, J., Puchtel, I.S. (2015) Copper isotope evidence for large-scale sulphide fractionation during Earth's differentiation. *Geochemical Perspectives Letters* 1, 53-64. https://doi.org/10.7185/geochemlet.1506

Shahar, A., Elardo, S.M., Macris, C.A. (2017) Equilibrium Fractionation of Non-traditional Stable Isotopes: an Experimental Perspective. *Reviews in Mineralogy and Geochemistry* 82, 65–83. https://doi.org/10.2138/rmg.2017.82.3

Shread, E.E., Chabot, N.L., Hamill, C.D., Ash, R.D., Corrigan, C.M. (2024) The crystallization of iron meteorites and the effect of troilite on trace element chemistry. *55th Lunar and Planetary Science Conference*, abstract #1024. https://www.hou.usra.edu/meetings/lpsc2024/pdf/1024.pdf

Williams, H.M., Archer, C. (2011) Copper stable isotopes as tracers of metal–sulphide segregation and fractional crystallisation processes on iron meteorite parent bodies. *Geochimica et Cosmochimica Acta* 75, 3166–3178. https://doi.org/10.1016/j.gca.2011.03.010

Xia, Y., Kiseeva, E., Wade, J., Huang, F. (2019) The effect of core segregation on the Cu and Zn isotope composition of the silicate Moon. *Geochemical Perspectives Letters* 12, 12-17. https://doi.org/10.7185/geochemlet.1928

Young, E.D., Galy, A., Nagahara, H. (2002) Kinetic and equilibrium mass-dependent isotope fractionation laws in nature and their geochemical and cosmochemical significance. *Geochimica et Cosmochimica Acta* 66, 1095–1104. https://doi.org/10.1016/S0016-7037(01)00832-8